The Limit of Magnetic-Shear Energy in Solar Active Regions
Short title: **Magnetic Energy Limit in Active Regions**

Ronald L. Moore[1], David A. Falconer[1, 2, 3], and Alphonse C. Sterling[1]
[1]Heliophysics and Planetary Science Office, ZP13, Marshall Space Flight Center, Huntsville, AL 35812, USA; ron.moore@nasa.gov
[2]Physics Department, University of Alabama in Huntsville, AL 35899, USA
[3]Center for Space Plasma and Aeronomic Research, University of Alabama in Huntsville, AL 35899, USA

ABSTRACT

It has been found previously, by measuring from active-region magnetograms a proxy of the free energy in the active region's magnetic field, (1) that there is a sharp upper limit to the free energy the field can hold that increases with the amount of magnetic field in the active region, the active region's magnetic flux content, and (2) that most active regions are near this limit when their field explodes in a CME/flare eruption. That is, explosive active regions are concentrated in a main-sequence path bordering the free-energy-limit line in (flux content, free-energy proxy) phase space. Here we present evidence that specifies the underlying magnetic condition that gives rise to the free-energy limit and the accompanying main sequence of explosive active regions. Using a suitable free energy proxy measured from vector magnetograms of 44 active regions, we find evidence that (1) in active regions at and near their free-energy limit, the ratio of magnetic-shear free energy to the non-free magnetic energy the potential field would have is of order 1 in the core field, the field rooted along the neutral line, and (2) this ratio is progressively less in active regions progressively farther below their free-energy limit. Evidently, most active regions in which this core-field energy ratio is much less than 1 cannot be triggered to explode; as this ratio approaches 1, most active regions become capable of exploding; and when this ratio is 1, most active regions are compelled to explode.

Key words: Sun: activity – Sun: surface magnetism – Sun: magnetic topology – Sun: coronal mass ejections (CMEs) – Sun: flares

1. INTRODUCTION

Observations, theory, and computational MHD modeling of solar flares and coronal mass ejections (CMEs) have established that these eruptions are magnetically driven: their energy comes from the magnetic field in which they happen, field that resides in the chromosphere and corona at the start of the eruption (e.g., Zirin 1988; Klimchuk 2001; Gopalswamy et al 2006). The strongest chromospheric and coronal magnetic fields that occur on the Sun are in large-sunspot active regions, and the greatest CME/flare eruptions are produced by certain of these active regions, those in which the magnetic field is extremely sheared and twisted (e.g., Zirin & Liggett 1987).

To be able to have a CME/flare eruption, an active region's chromospheric and coronal field must have free energy. That is, it must be deformed relative to its potential-field configuration, the configuration in which the field has no curl and hence no electric current. The potential-field configuration is the configuration of minimum magnetic energy, the configuration in which the field has no free energy.

Active regions are evidently produced by the emergence of the tops of buoyant Ω loops of toriodal magnetic flux ropes that are generated near the base of the Sun's convection mantel by the global dynamo process (e.g, Charbonneau 2005). The result is that any active region is grossly comprised of one or more bipolar magnetic arcades, each of which arches into the low corona and is centered on its polarity inversion line (neutral line) in the active region's photospheric magnetic flux (e.g., Moore 1992). This paper is focused on the field in the cores of an active region's dominant magnetic arcades. This is the field rooted near the active region's major neutral lines, the neutral lines between the active region's major domains of opposite-polarity flux. We refer to this field as the active region's "core field."

In most active regions that produce CME/flare eruptions, photospheric vector magnetograms and chromospheric and coronal images show that the free energy is concentrated in the core field in the form of non-potential shear and twist (e.g., Moore & Rabin 1985; Moore et al 1987; Zirin 1988; Canfield et al 1999). It is also observed that active regions that display obvious core-field sigmoidal shear and twist in coronal X-ray and EUV images are much more prone to have CME/flare eruptions than active regions that display no obvious core-field contortion (Canfield et al 1999; Sterling et al 2000). Thus, the qualitative field morphology observed in vector magnetograms and images of active regions indicates that the active regions having the most free magnetic energy are the most CME/flare-productive. Quantitatively, the level of free magnetic energy at which an active region becomes compelled to have a CME/flare eruption remains undetermined. This paper infers this level from measurements of active-region magnetograms.

In Falconer et al (2009), to explore the relation of the CME/flare productivity of active regions to their free energy and magnetic flux, we measured two whole-active-region magnetic quantities from SOHO/MDI line-of-sight magnetograms of active regions viewed on the central face of the Sun. One of the two quantities measured from each active-region magnetogram was a proxy for the active region's free-energy content, and the other was an approximation of the active region's magnetic-flux content. We found that the distribution of active regions in the phase space of Log (free-energy proxy) versus Log (flux content) is a diagonal cloud of positive slope (as will be shown in Section 3). This demonstrates that of course having more magnetic flux allows an active region to have more free energy. Of more importance, the cloud has a rather sharp diagonal upper edge. This shows that active regions have a rather sharp upper limit to their free energy, and that this maximum attainable free energy increases with flux content. This suggests that there is some uniform condition that sets the free-energy limit for active regions of all sizes in flux content. Because, instead of the free energy, only a proxy of the free energy was measured and plotted, the free-energy-limit edge of the cloud does not directly give either the limiting amount of free energy or the increase in this amount with increasing flux content. This paper finds empirical evidence pointing to the maximum free magnetic energy an active region can hold being of the order of the non-free magnetic energy of the active region's field were the field fully relaxed to its potential-field configuration.

2

2. EXPLOSIVE ACTIVE REGIONS

2.1. Example Explosive Active Region

The first panel of Figure 1 is a vector magnetogram of a largely bipolar active region, NOAA AR 9026, observed at 19:19 UT on 2000 June 6 by the Marshall Space Flight Center (MSFC) vector magnetograph. This is a sub field of view from the full magnetogram, which covered all of AR 9026 and much of a contiguous active region (AR 9030) on the east side of AR 9026. This close-up view is centered on the main neutral line of AR 9026 and covers most of the flux in AR 9026. About four hours earlier, the magnetic field in AR 9026 exploded, producing the halo CME and GOES X-class flare shown in the top part of Figure 2. In the bottom part of Figure 2, the field of view of Figure 1 is outlined on an MDI photospheric intensity image and on an MDI line-of-sight magnetogram. This shows that the vector magnetogram in Figure 1 is centered on a large bipolar δ sunspot and that the main neutral line runs through the δ sunspot.
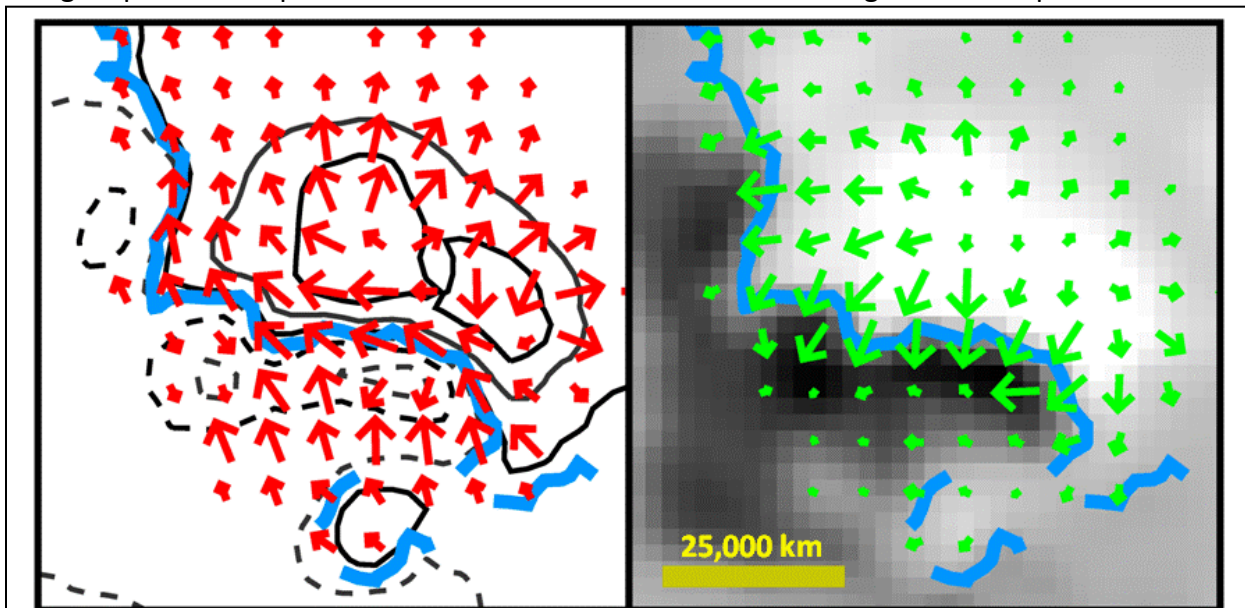

Figure 1. Deprojected MSFC vector magnetogram of the magnetic field in and around the large δ sunspot in NOAA Active Region 9026 on 2000 June 6, showing the extreme shear in the field near the neutral line. In the first panel, the solid (dashed) contours map the strength of the upward (downward) vertical component of the observed field, and the red arrows show the strength and direction of the horizontal component of the observed field. In the second panel, the lighter (darker) shades of gray map the strength of the upward (downward) vertical component of the observed field, and the green arrows show the strength and direction of the horizontal component of the potential field computed from the vertical-field component of the magnetogram. In both panels, the blue curves show the strong-field intervals of the neutral line, the intervals on which the potential field is stronger than 150 G.

The vector magnetogram in Figure 1 displays the vertical and horizontal components of the vector magnetic field observed in the photosphere. The original magnetogram from the vector magnertograph is a plane-of-the sky map of the line-of-sight and transverse components of the

field, the components directly observed by the magnetograph. After resolution of the 180° ambiguity of the transverse-field direction in the original magnetogram, the vector magnetogram in Figure 1 was obtained by deprojecting the original magnetogram to disk center (Falconer et al 2006). That is, this version of the magnetogram was obtained by transforming the original magnetogram to display the vector field as though the magnetograph observed the active region directly from above, or, equivalently, as though the active region were observed at disk center. Active-region vector magnetograms that have been transformed to their vertical and horizontal components in this way, we refer to as deprojected vector magnetograms.
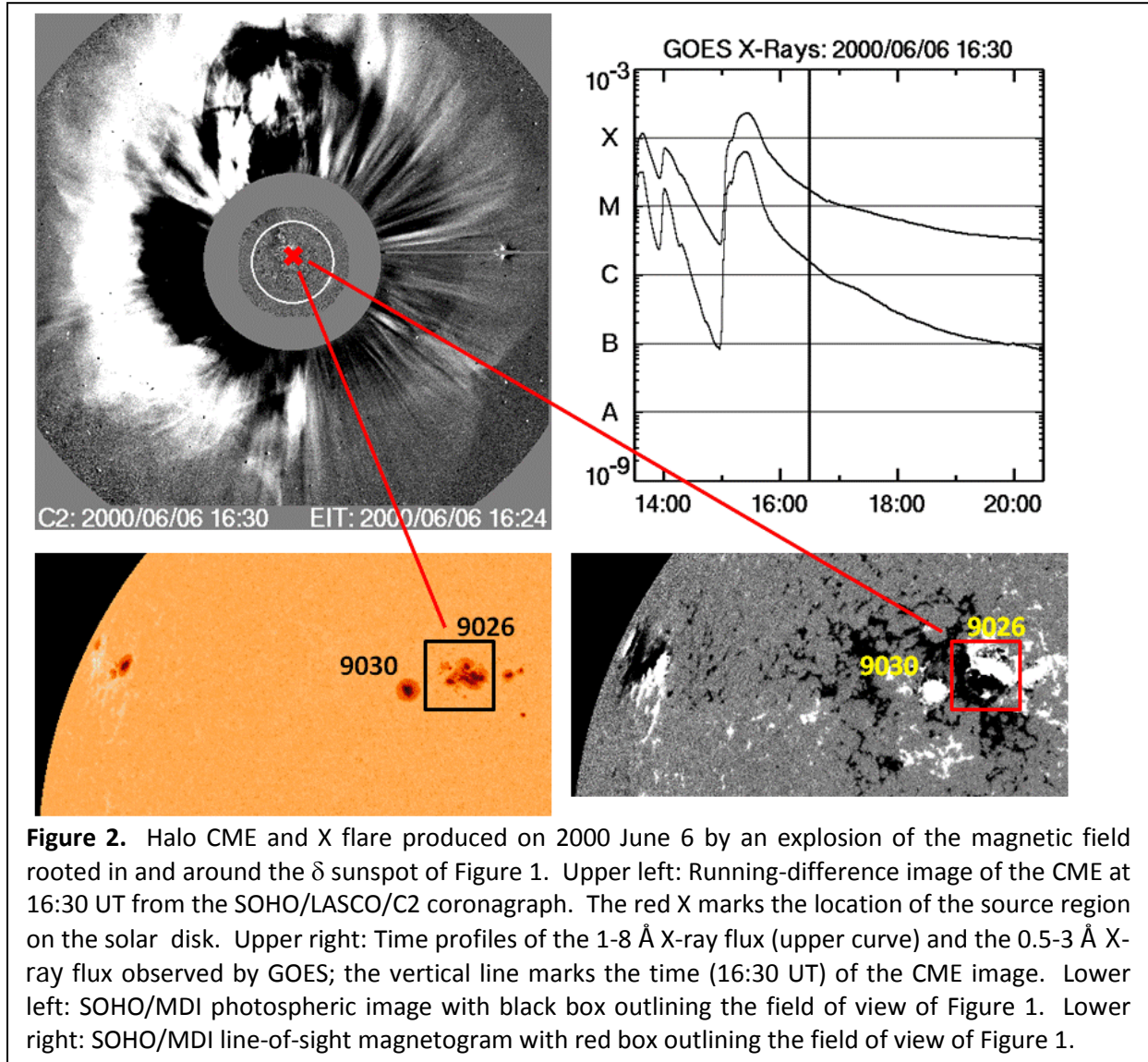

Figure 2. Halo CME and X flare produced on 2000 June 6 by an explosion of the magnetic field rooted in and around the δ sunspot of Figure 1. Upper left: Running-difference image of the CME at 16:30 UT from the SOHO/LASCO/C2 coronagraph. The red X marks the location of the source region on the solar disk. Upper right: Time profiles of the 1-8 Å X-ray flux (upper curve) and the 0.5-3 Å X-ray flux observed by GOES; the vertical line marks the time (16:30 UT) of the CME image. Lower left: SOHO/MDI photospheric image with black box outlining the field of view of Figure 1. Lower right: SOHO/MDI line-of-sight magnetogram with red box outlining the field of view of Figure 1.

In the second panel of Figure 1, the green arrows display the strength and direction of the photospheric horizontal component of the potential field computed from the vertical-field component of the deprojected full MSFC vector magnetogram. For clarity, these vectors are displayed for only 1 out of 9 pixels. The green arrows show that at the main neutral line the direction of the potential field is nearly orthogonal to the neutral line, both inside and outside

of the δ sunspot. In the first panel of Figure 1, the red arrows display the observed horizontal-field component of the deprojected magnetogram, and the contours display the vertical-field component. The reds arrows and the green arrows together show that the magnetic arcade rooted in and around the δ sunspot had magnetic shear concentrated in its core field in the characteristic manner of explosive solar magnetic arcades: near the main neutral line the horizontal direction of the field is nearly orthogonal to the potential field direction. That is, in this arcade, as in most other explosive arcades, the core field is so strongly sheared relative to the potential field that its direction is roughly parallel to the neutral line (e.g., Moore & Sterling 2006).

2.2. Standard Model for CME/Flare Eruptions

Practically all major CME/flare eruptions are made by the explosion of a sheared-core magnetic arcade that is basically of the form of the one that exploded in our above example CME/flare eruption (e.g., Moore & Sterling 2006; Moore et al 2007; Moore et al 2011). Figure 3 is our cartoon depiction of the rudiments of the three-dimensional form of the magnetic field in these explosive sheared-core magnetic arcades and the field's transformation as it explodes in the production of a CME and flare (Moore et al 2001). This basic picture for the form of the field and its reconnection in a CME/flare eruption was first proposed by Hirayama (1974) and has since been adapted by many others (e.g., Kopp & Pneumann 1976; Heyvaerts et al 1977; Moore & LaBonte 1980; Sturrock et al 1984; Shibata et al 1995; Shibata 1998; Forbes 2000; Roussev et al 2003; Gibson et al 2004; Qiu et al 2004; Wang 2006; Aulanier et al 2010).

The first panel of Figure 3 shows the arcade prior to eruption onset. The core field is strongly sheared and contorted from the form of the potential field so that is has an overall sigmoidal shape. The sigmoid runs along the neutral line through the arcade and curves out of each end of the arcade. If, as in Figure 3, the sense of the shear is left-handed, the sigmoid has the shape of an inverse S. The core-field sigmoid is S-shaped in arcades in which the shear is right-handed. Outside the swath of strongly-sheared core field, the shear in the field decreases with increasing distance from the neutral line, so that the field in the outer envelope of the arcade arches over the neutral line much more nearly in the direction of the potential field than in the direction of the core field. The pre-eruption arcade often holds a filament of chromospheric-temperature plasma in its core as indicated in the first panel of Figure 3. The filament plasma is suspended in what amounts to a flux rope (not shown in Figure 3) that runs the length of the sigmoid and is horizontal or mildly dipped through the middle of the arcade. The flux rope floats in the core field above the neutral line in the middle of the arcade and has its feet in the ends of the sigmoid.

In a pre-eruption active-region arcade such as depicted in Figure 3, because the core field is nearly orthogonal to the potential-field direction, the core field's magnetic energy is nearly all free energy. In a CME/flare eruption some of this free energy is explosively released. Because the magnetic field in the chromosphere and corona in active regions is much stronger than the plasma, when the field is in static equilibrium (not exploding), it is in a nearly plasma-force-free equilibrium configuration. Anywhere the field lines are inwardly curved in an active-region arcade, the outward push on the field by the gradient in the magnetic pressure is balanced by the inward pull of the magnetic-tension stress in the field (e.g., Cowling 1957). In the potential-
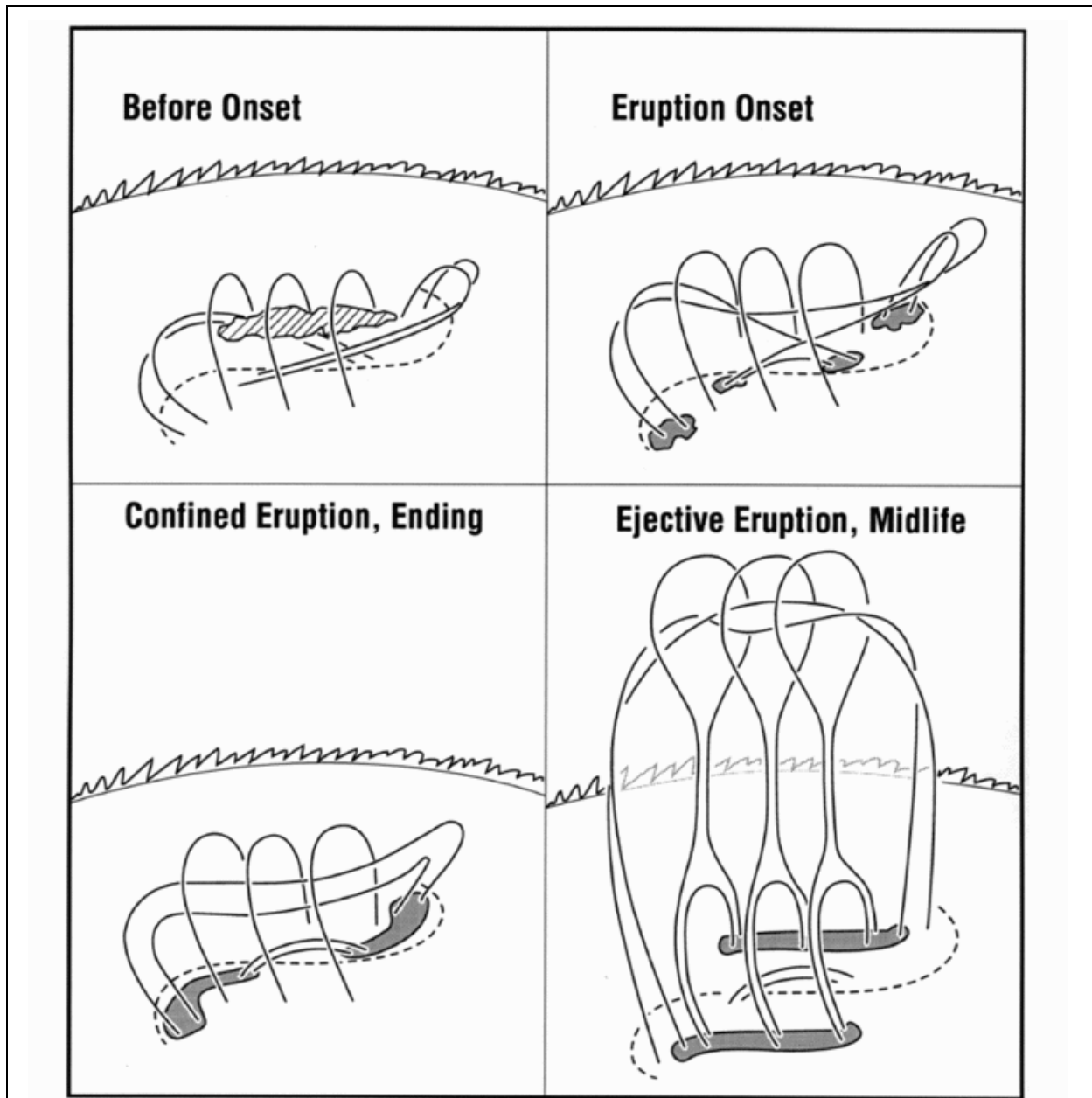
Figure 3. The typical three-dimensional configuration and reconnection of the magnetic field before and during the field's explosion in major CME/flare eruptions (from Moore et al 2001). The explosive sheared-core arcade field is depicted here near the limb. The solid curves are field lines; the dashed curve is the arcade's neutral line on the Sun's surface; and the shaded areas are flare ribbons at the feet of reconnected field lines. The third panel shows the end of a confined explosion, a "failed-CME" eruption.

field configuration, the force-free-field configuration of minimum (zero) free energy, the field lines are everywhere inwardly curved. The strongly-sheared core field in a pre-eruption active-region arcade has much less inward curvature than the potential field would have, and can even have some outward curvature in the middle of the arcade. So, locally, compared to the potential field, the sheared core field is much less kept from expanding by its own magnetic tension. Instead, the core field is chiefly held in check by the counteracting pull of the magnetic

6

tension in the legs of the envelope field. Gradually increasing the free energy by gradually increasing the shear in the core field gradually inflates the entire arcade field, puffing out the top and sides of the arcade (e.g., Lynch et al 2008). When the arcade has enough free energy from shear in its core field, the equilibrium of the inflated arcade can be lost or broken by some trigger mechanism, and the core-field flux rope starts erupting. The eruption then grows explosively and produces a CME and flare via reconnection that is below the erupting core-field flux rope, adds more flux to the flux rope, and further unleashes it to expand and erupt out in the manner sketched in Figure 3.

The specific trigger mechanism that initiates any particular eruption depends on the specifics of the arrangement and evolution of the field in the explosive arcade and of any field in which the explosive arcade is situated. The eruptive arcade depicted in Figure 3 is shown standing alone with no other magnetic field around it, whereas our example observed eruptive-arcade field in Figures 1 and 2 is in the western bipolar domain of the quadrupolar flux arrangement of the two merged active regions, AR 9026 and AR 9030, labeled in the magnetogram in Figure 2. In this more complex magnetic setting, there are three basic mechanisms that might trigger our example sheared-core-arcade field to erupt. An eruption might be trigged by any one of these mechanisms acting alone, or by any two or all three acting in concert (e.g., Moore & Sterling 2006). The three triggering mechanisms are: onset of internal tether-cutting reconnection low in the sheared core field, e.g., as depicted in Figure 3 (Moore & Roumeliotis 1992); onset of breakout reconnection (a.k.a. external tether-cutting reconnection) between the top of the arcade and contiguous oppositely-directed field, not shown in Figure 3 (Antiochos 1998); and onset of an ideal MHD instability, such as kink instability of the flux rope, in the absence of any initial reconnection (Rust & Kumar 1996; Forbes 2000).

The present paper is not concerned with eruption trigger mechanisms per se. Instead, this paper deals with the level of magnetic-shear free energy at which active regions become capable of being triggered to have a CME/flare eruption, and with the level of magnetic-shear free-energy at which they become compelled to have CME/flare eruptions.

3. FREE-ENERGY LIMIT AND MAIN SEQUENCE OF EXPLOSIVE ACTIVE REGIONS

The present paper stems from the Falconer et al (2009) paper mentioned in Section 1. We now lay out the measurements and results from that paper that are used in this paper.

3.1. Active-Region Magnetogram Measures

Because we are especially interested in the magnetic conditions in active regions that produce the most powerful CME/flare eruptions, and because these eruptions are produced by contorted magnetic fields in large-sunspot active regions, in Falconer et al (2009), in our previous related work, and in the present work, we measure only magnetograms of what we define to be strong-field active regions. We define strong-field active regions to be those in which, in a deprojected vector magnetogram, the total length of the strong-field intervals of the neutral lines is at least 75% of the active region's span given by the square root of the total area of the magnetogram in which the strength of the vertical component of the field exceeds 100

G. We define the strong-field neutral-line intervals to be those on which the horizontal component of the potential field computed from the vertical-field component of the magnetogram exceeds 150 G. We have found that practically all active regions having substantial sunspots are strong-field active regions by this definition.

If we had vector magnetograms of the force-free field in the chromosphere in active regions, we could, via the virial theorem for force-free magnetic fields, directly measure from the vector magnetogram the total free energy in an active region's magnetic field above the height of the magnetogram (e.g., Low 1982; Gary et al 1987). That method cannot be used yet because all past and present routinely produced vector magnetograms are of the strongly non-force-free roots of the field in the photosphere. Instead, we and several other researchers have separately devised a variety of photospheric-magnetogram measures that are proxy measures of an active region's free magnetic energy, measures of aspects of the magnetogram that are signatures of the free energy stored in the active region's field above the photosphere (Falconer 2001; Falconer et al 2002, 2003, 2006, 2008; Leka & Barnes 2003a,b: Cui et al 2006; Jing et al 2006; Georgoulis & Rust 2007; Schrijver 2007). These proxy measures do not have units of energy, but each increases with increasing free energy in an active region's field, that is, with increasing deformation of the field from the potential-field configuration.

There are five active-region magnetogram measures that are especially pertinent to the Falconer et al (2009) paper. Three are measured from a deprojected vector magnetogram. One of these (symbolized by Φ) is a measure of the active region's total magnetic flux, and the other two (symbolized by WL_{SS} and WL_{SG}) are proxy measures of the active region's free magnetic energy. The remaining two magnetogram measures are measured from a line-of-sight magnetogram or from the line-of-sight component of a non-deprojected vector magnetogram. One of these (symbolized by $^L\Phi$) is an approximation of Φ, and the other (symbolized by $^LWL_{SG}$) is an approximation of WL_{SG}. For each of these five measures, the measurement uncertainty is determined from the uncertainties in the measured magnetogram as described in Falconer et al (2008).

The five magnetogram measures are defined as follows:

1. The flux-content measure Φ is the area integral of the unsigned vertical flux density $|B_z|$ over all areas of the active region's deprojected vector magnetogram having $|B_z| > 100$ G.

2. The flux-content measure $^L\Phi$ is the approximation of Φ that is measured from a line-of-sight magnetogram instead of from the vertical-field component of a deprojected vector magnetogram. It is the area integral of the unsigned line-of-sight flux density $|B_{LOS}|$ over all areas of the active region's line-of-sight magnetogram having $|B_{LOS}| > 100$ G.

3. The free-energy proxy WL_{SS} is the shear-weighted length of strong-field neutral line in the active region. It is the line integral of the magnetic shear angle on all strong-field intervals of all neutral lines in the active region's deprojected vector magnetogram. The shear angle is the angle between the observed horizontal field component and the horizontal component of the potential field computed from the vertical-field component of the deprojected magnetogram.

4. The free-energy proxy WL_{SG} is the gradient-weighted length of strong-field neutral line in the active region. It is the line integral of the horizontal gradient of the vertical-field flux density B_z on all strong-field intervals of all neutral lines in the active region's deprojected vector magnetogram.
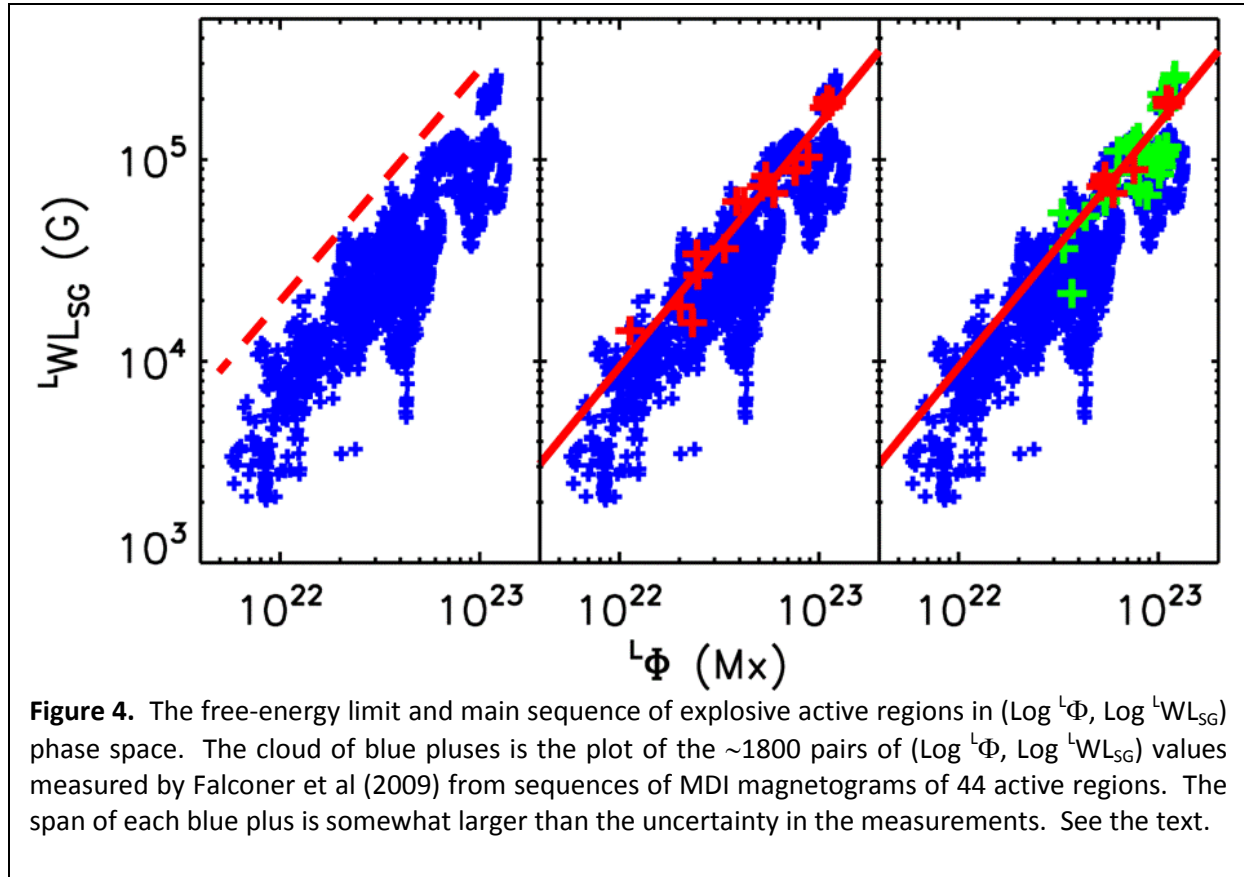
5. The free-energy proxy $^{\llcorner}WL_{SG}$ is the approximation of WL_{SG} that is measured from a line-of-sight magnetogram instead of from the vertical-field component of a deprojected vector magnetogram. It is the line integral of the transverse gradient of the line-of-sight flux density B_{LOS} on all strong-field intervals of all neutral lines in the active region's line-of-sight magnetogram. We define the strong-field neutral-line intervals of a line-of-sight magnetogram to be those on which the transverse component of the potential field computed from the line-of-sight magnetogram exceeds 150 G.

Each of the magnetogram measures, WL_{SS}, WL_{SG}, and $^{\llcorner}WL_{SG}$, is a proxy measure of an active region's free magnetic energy by virtue of (1) the observed strong correlation between magnetic shear and vertical-field horizontal gradient at strong-field neutral lines (Falconer et al 2003), and (2) the observed strong correlation between the amount of magnetic shear along the neutral line and the net electric current arching over the neutral line in bipolar active regions (Falconer et al 2006). Because the net electric current in a bipolar active region directly corresponds to the free energy, it is certainly a proxy measure of the active region's free energy. Hence, because we have found WL_{SG} to be strongly correlated with WL_{SS} in both bipolar and multipolar active regions, and have found WL_{SS} and WL_{SG} to be strongly correlated with the net electric current in bipolar active regions, we conclude that each of the magnetogram measures, WL_{SS}, WL_{SG}, and $^{\llcorner}WL_{SG}$, is a proxy measure of the free energy in both bipolar and multipolar active regions.

In Falconer et al (2006, 2008), we measured MSFC vector magnetograms of strong-field active regions that were within $\sim 0.5 R_{Sun}$ ($\sim 30°$) from disk center, and examined the correlation of active-region CME productivity with active-region magnetic flux content and with various proxies of active-region free magnetic energy. Of particular importance for the Falconer et al (2009) paper, we examined these correlations (a) for the flux content Φ and the free-energy proxies WL_{SS} and WL_{SG} measured from the deprojected magnetograms, and (b) for the approximations to Φ and WL_{SG}, $^{\llcorner}\Phi$ and $^{\llcorner}WL_{SG}$, measured directly from the non-deprojected observed magnetograms. We found three key results pertinent to the Falconer et al (2009) paper: for strong-field active regions measured when they are within $0.5 R_{Sun}$ from disk center, (1) $^{\llcorner}\Phi$ approximates Φ to within a factor of 2, (2) for CME prediction, WL_{SG} works as well as WL_{SS} (the CME-prediction success rate for each was $\sim 80\%$), and (3) $^{\llcorner}WL_{SG}$ approximates WL_{SG} to within a factor of ~ 2, and for CME prediction, $^{\llcorner}WL_{SG}$ works as well as WL_{SG} (for our sample of 41 active regions that were strictly within $0.5 R_{Sun}$ from disk center, the CME-prediction success rate for $^{\llcorner}WL_{SG}$ was $\sim 85\%$). It is these three results that for the Falconer et al (2009) paper permitted us to use $^{\llcorner}\Phi$ and $^{\llcorner}WL_{SG}$ measured from MDI line-of-sight magnetograms to study CME/flare productivity in relation to the distribution of active regions in (flux content, free-energy proxy) phase space.

3.2. Free-Energy Limit

The (Log $^{\llcorner}\Phi$, Log $^{\llcorner}WL_{SG}$) phase-space distribution found by Falconer et al (2009) from 44 full-grown sunspot active regions is outlined by the diagonal blue cloud of measured (Log $^{\llcorner}\Phi$, Log $^{\llcorner}WL_{SG}$) points in Figure 4. The passage of each of the 44 active regions across the 30°-radius

Figure 4. The free-energy limit and main sequence of explosive active regions in (Log $^L\Phi$, Log $^LWL_{SG}$) phase space. The cloud of blue pluses is the plot of the ~1800 pairs of (Log $^L\Phi$, Log $^LWL_{SG}$) values measured by Falconer et al (2009) from sequences of MDI magnetograms of 44 active regions. The span of each blue plus is somewhat larger than the uncertainty in the measurements. See the text.

central face of the Sun was tracked in the full-disk MDI magnetograms, which usually had a 96-minute cadence (15/day), and $^L\Phi$ and $^LWL_{SG}$ were measured from each magnetogram of each active region. This yielded ~1800 (Log $^L\Phi$, Log $^LWL_{SG}$) points, the population of the blue cloud in Figure 4. (The data points plotted here in Figure 4 are the ones plotted in Figure 1 of Falconer et al (2009), but here we have switched the axes.)

In the first plot in Figure 4, only the cloud of ~1800 (Log $^L\Phi$, Log $^LWL_{SG}$) points is shown, with no indication of the phase-space location of active regions when they had CME and/or flare eruptions. The diagonal upper edge of the cloud is considerably less ragged than the lower edge. The straight dashed red line along the upper edge has a slope of about 1.3. This line shows that the cloud's upper edge roughly tracks a power-law line along which the free-energy proxy $^LWL_{SG}$ increases as $^L\Phi^{1.3}$. Thus, the first plot in Figure 4 graphically shows that the free energy that an active region can attain has a rather abrupt upper limit that is largely determined by how much magnetic field the active region has, its total magnetic flux.

3.3. Main Sequence of Explosive Active Regions

In this paper, the term "major flare" refers to any flare that produces a sufficiently strong burst of soft X-ray emission, a burst of class M or X in GOES X-ray flux. Many of the 44 active

regions tracked and measured for the Falconer et al (2009) paper produced one or more CMEs and/or major flares during their passage across the 30°-radius central disk. For each of the CMEs, the (flux content, free-energy proxy) data point from the source active region's magnetogram nearest in time to the start of the CME eruption is marked by a red cross in the second plot in Figure 4. Similarly, in the third plot in Figure 4, for each GOES X-class flare produced by the 44 active regions during central-disk passage, the data point from the flaring active region's magnetogram nearest in time to the start of the flare is marked by a red cross, and for each GOES M-class flare produced during central-disk passage, the data point from the flaring active region's magnetogram nearest in time to the start of that flare is marked by a green cross. Most of the CME points in the second plot in Figure 4 are either an X-flare point or an M-flare point in the third plot because the flare that was produced along with the CME a la Figure 3 was an X or M flare. For the few CME points that are not X-flare of M-flare points, the co-produced flare was only a C flare, that is, was weaker than an M flare in GOES X-ray flux. The CME points and the X-flare points are distributed in a band along the diagonal upper edge of the blue cloud. The M-flare points are also concentrated along the upper edge of the cloud, but scatter farther below it than the points for the X flares and CMEs. In the second plot in Figure 4, the solid red line is the least-squares linear fit to the CME points. This CME-fit line is also shown in the third plot in Figure 4, confirming that the X-flare points and the CME points are concentrated in the same band bordering the upper edge of the blue cloud. Thus, Figure 4 shows that most CMEs and major flares are produced by active regions in which the magnetic field has close to its maximum attainable free energy. That is, there is a main sequence of explosive active regions in (Log $^L\Phi$, Log $^L WL_{SG}$) phase space, the active regions that border the free-energy-limit upper edge of the blue cloud. This result indicates that the magnetic field of an active region of any given magnetic size $^L\Phi$ becomes increasingly more explosive as the field's free energy approaches its upper limit.

For the Falconer et al (2009) sample of 44 active regions and their CMEs, M flares, and X flares produced during central disk passage, as Figure 4 shows, the CMEs were produced only by active regions having magnetic flux content $^L\Phi$ greater than 1 x 10^{22} Mx, the M flares were produced only by active regions having $^L\Phi$ > 3 x 10^{22} Mx, and the X flares were produced only by active regions having $^L\Phi$ > 5 x 10^{22} Mx. This indicates that no matter how explosive smaller active regions (i.e., smaller in magnetic flux) may become as their free energy approaches its upper limit, the biggest explosions they can have are not as big as the biggest explosions that larger active regions can have. Presumably, this is simply because the free-energy limit is lower for smaller active regions than for larger active regions.

From Figure 4, active regions that are large enough to produce M and X flares evidently become increasingly more productive of major flares and CMEs as their free energy approaches its upper limit. From this observation, Falconer et al (2009) proposed that the general physical cause of the free-energy limit is that the rate at which an active region's free energy is burned down by CMEs, flares, and coronal heating steeply increases with increasing free energy. The maximum free energy that active regions of a given flux content can attain is then the level of free energy at which the burn-down rate equals the maximum rate at which convective driving of the roots of an active region's magnetic field in and below the photosphere can pump free energy into the field above the photosphere. In support of this hypothesis, Falconer et al

(2009) showed that for the active regions in their sample that were large enough to produce X flares, the rate of energy output in the GOES 1-8 Å X-ray band by M and X flares increases increasingly more steeply with distance in the direction of increasing free energy normal to the CME-fit line in Figure 4 as this line is crossed and the free-energy-limit line is approached. On the basis of this result, Falconer et al (2009) named the band of active regions along the upper edge of the cloud the main sequence of explosive active regions in (flux content, free energy) phase space by analogy with the main sequence of hydrogen-burning stars in (mass, luminosity) phase space. In both cases, the main sequence is the locus in phase space where there is a balance of rate of gain of energy and rate of loss of energy, balance of rate of gain and rate of loss of thermal energy in the case of the main sequence of stars and balance of rate of gain and rate of loss of free magnetic energy in the case of the main sequence of explosive active regions.

Hydrogen-burning fusion is the underlying process that for stars of all masses on the main sequence sustains the equilibrium of rate of gain and rate of loss of thermal energy: hydrogen-burning fusion is the underlying cause of the main sequence. Does the main sequence of explosive active regions have an analogous uniform underlying cause? Throughout the magnetic-flux-content range of active regions, is there a uniform condition of the magnetic field that results in the free-energy limit and the concomitant main sequence of explosive active regions? In other words, is there a uniform magnetic condition for active regions of any size that renders the magnetic field explosive enough to limit its free energy? In Figure 4, the power-law straight-line increase of maximum free-energy proxy $^{\llcorner}WL_{SG}$ with increasing flux content $^{\llcorner}\Phi$ (the straight-line increase shown by the free-energy-limit line in the first plot) suggests that the answer to this question is yes. Whether there is indeed a uniform condition and, if there is, what that condition is cannot be determined from the data in Figure 4 alone. This paper presents empirical evidence that there is a uniform underlying magnetic condition that results in the free-energy limit and explosive main sequence. This evidence suggests that the uniform condition is the maximum attainable ratio of free energy of the active region's magnetic field to the non-free energy the field would have were it fully relaxed to its potential-field configuration, and that this ratio is of order 1.

4. HYPOTHESIS

As we noted in Section 1, an active region is largely composed of one or more major bipolar magnetic arcades, each of which is presumably the emerged top of an Ω-loop flux rope that buoyantly rises up from east-west toroidal magnetic field near the base of the convection zone. Among the most explosive active-region magnetic arcades are those rooted in large δ sunspots such as in the example explosive active region in Section 2. Such δ sunspots are basically two opposite-polarity sunspots of comparable size, crammed together along the neutral line running through the middle of the δ sunspot. Vector magnetograms and high-resolution photospheric, chromospheric, and coronal images show that the field rooted along the neutral line, the core field of the arcade, is extremely sheared. As in the example δ sunspot in Figures 1 and 2, the direction of the polarity axis of a δ sunspot, the direction roughly orthogonal to the

neutral line, is typically rotated ~90° or more from the roughly east-west direction of normal bipolar active regions (Tanaka 1991). These characteristics of δ sunspots suggest that the magnetic arcade rooted in a δ sunspot is the emerged kinked top of an Ω loop of a flux rope that had so much axial twist that it was kink-unstable, causing the Ω loop to writhe into a kink as it rose through the convection zone. Fan et al (1999) found support for this scenario from MHD modeling of the buoyant rise of active-region-size flux ropes that at the base of the convection zone had uniform axial twist.

In the MHD simulations of Fan et al (1999), at the start of a simulation, the model flux rope is at the base of the convection zone, horizontal, and has cylindrical symmetry and uniform axial twist. The twist is axial and uniform in that the field lines wind about the axis on cylindrical surfaces and all field lines in the flux rope have the same rate of rotation with distance along the axis: $B_\theta/B_x = \alpha r$, where B_x is the axial component of field, B_θ is the azimuthal component, r is the radial distance from the axis, and the twist parameter α is constant, the uniform rate of rotation in radians per unit length. In the simulations, the flux ropes having more than a critical amount of axial twist kinked as the Ω loop rose through the convection zone, by spontaneous conversion of the excess axial twist into the writhe twist of the kink.

The greater a flux rope's axial twist, the greater the ratio of the azimuthal component to the axial component and the greater the ratio of azimuthal-field energy to axial-field energy in the flux rope. The flux rope's axial-field energy is analogous to an active region's potential-field energy, and the flux rope's azimuthal-field energy is analogous to an active region's free magnetic energy. A flux rope that has no axial twist has no azimuthal-field energy for kinking, and a potential-field active region has no free magnetic energy for erupting. Only flux ropes with enough twist are kink-unstable, and only active regions with enough free magnetic energy are explosive.

Both perturbation analysis of the kink instability of axially-twisted flux ropes and MHD simulations find that the flux rope becomes kink-unstable when the axial twist becomes great enough that the azimuthal-field energy becomes comparable to the axial-field energy (Fan et al 1999). This implies that in any kinked Ω-loop flux rope that emerges to become a δ-sunspot arcade, the ratio of azimuthal-field energy to axial-field energy is of order 1 before the kinked Ω loop emerges from the convection zone. This suggests to us that the ratio of free magnetic energy to potential-field energy in δ-sunspot magnetic arcades is of order 1. Active region's that have large δ sunspots are members of the explosive main sequence due to having extremely sheared core fields and correspondingly extremely strong horizontal gradients of the vertical field at the neutral line through the δ sunspot, which gives them values of the free-energy proxy $^LWL_{SG}$ near the upper limit.

From the above considerations, we hypothesize that in all active regions that are near the free-energy-limit line in (Log $^L\Phi$, Log $^LWL_{SG}$) phase space, i.e., in all active regions in the explosive main sequence regardless of magnetic size and whether or not they have δ sunspots, the free magnetic energy is of order the non-free magnetic energy the field would have were it in its potential-field configuration. That is, our hypothesis is that this level of free magnetic energy relative to the potential-field energy is the uniform magnetic condition underlying the free-energy limit and explosive main sequence of active regions.

13

5. RATIO OF FREE MAGNETIC ENERGY TO POTENTIAL-FIELD ENERGY IN AN ACTIVE REGION: A PROXY MEASURE

We test our hypothesis with a proxy measure of the ratio of the free magnetic energy in an active region's magnetic field to the non-free energy the field would have were it relaxed to its zero-free-energy potential-field configuration.

At each point on a neutral line in a deprojected active-region vector magnetogram, the vector of the observed field and the vector of the potential field are both horizontal, and the observed field vector is at some angle θ to the potential-field vector. The angle θ is the horizontal magnetic shear angle defined in Section 3.1, the angle by which the observed field on the neutral line is horizontally sheared relative to the potential field. So, at each point on a neutral line, the observed field vector has no vertical component and can be decomposed into two orthogonal horizontal components, parallel and perpendicular to the potential field: $^{||}B_{obs} = B_{obs} \cos \theta$ and $^{\perp}B_{obs} = B_{obs} \sin \theta$, where B_{obs} is the magnitude of the observed field, and $^{||}B_{obs}$ and $^{\perp}B_{obs}$ are the magnitudes of the components parallel and perpendicular to the potential field. When $\theta = 0°$, the observed field has no horizontal shear and is entirely parallel to the potential field ($^{\perp}B_{obs}/^{||}B_{obs} = 0$). As θ increases from $0°$, the observed field has increasingly greater horizontal shear, $^{\perp}B_{obs}$ increases from 0, and $^{||}B_{obs}$ decreases until at $\theta = 90°$ the observed field is entirely orthogonal to the potential field ($^{||}B_{obs} = 0$). We name $^{\perp}B_{obs}$ the horizontal-shear component of the observed field on the neutral line, and name $^{||}B_{obs}$ the potential-field-direction component. The energy density of the horizontal-shear component ($B_{obs} \sin \theta)^2/8\pi$ we call the magnetic-shear energy density on the neutral line.

With the above definitions in hand, we are now ready to define an alternative proxy measure of the free energy in an active region's magnetic field, one that is analogous to our free-energy proxy WL_{SS} defined in Section 3.1. WL_{SS} is the shear-weighted length of strong-field neutral line in an active region's deprojected vector magnetogram: $WL_{SS} \equiv \int \theta \, dl$, where θ is the shear angle and l is length along the strong-field intervals of the neutral lines. As discussed in Section 3.1., WL_{SS} is a proxy measure of the total free magnetic energy in an active region by virtue of the free energy in active regions being concentrated in the core field in the form of horizontal shear in this field. For the same reason, the following neutral-line measure should be correlated with the total free energy at least as strongly as WL_{SS}. We call this free-energy proxy the shear-energy-density-weighted length of strong-field neutral line in the active region, and denote it by WL_{SSED}. It is the line integral of the magnetic-shear energy density on the strong-field intervals of the active region's neutral lines: $WL_{SSED} \equiv \int [(B_{obs} \sin \theta)^2/8\pi] \, dl$. In this proxy measure of the free energy, we use only the horizontal-shear component of the observed field ($B_{obs} \sin \theta$). We exclude the potential-field-direction component ($B_{obs} \cos \theta$) because it decreases with increasing core-field shear.

Directly corresponding to the free-energy proxy WL_{SSED} measured from the observed field, there is an analogous neutral-line measure of the potential field, a neutral-line measure that is a proxy measure of the active region's potential-field energy in the same way that WL_{SSED} is a proxy measure of the active region's free energy. We call this measure the potential-field-energy-density-weighted length of strong-field neutral line in the active region, and denote it by WL_{SPED}. It is the line integral of the energy density of the potential field on the strong-field

intervals of the active region's neutral lines: $WL_{SPED} \equiv \int[(B_{pot})^2/8\pi]\,dl$, where B_{pot} is the strength of the potential field.

The ratio of the shear-energy-density-weighted neutral-line length to the potential-field-energy-density-weighted neutral-line length, WL_{SSED}/WL_{SPED}, is a proxy measure of an active region's ratio of free magnetic energy to potential-field energy. We conjecture that this proxy energy ratio is of the order of the active region's actual ratio of free energy to potential-field energy. In any case, by construction, WL_{SSED}/WL_{SPED} approximates to order of magnitude the ratio of magnetic-shear energy to potential-field energy in the sum of the intervals of the active region's core field that envelop the strong-field intervals of the active region's neutral lines.

6. RESULTS

6.1. Core-Field Energy-Ratio Limit

For each of the 44 active regions that were tracked and measured in MDI line-of-sight magnetograms for the Falconer et al (2009) paper, we have an MSFC vector magnetogram of the active region when it was within ~30° of disk center. From the deprojected vector magnetogram of each active region, we have measured the flux content Φ, the free-energy proxy WL_{SSED}, and the potential-field energy proxy WL_{SPED}. For these 44 active regions, Figure 5 shows the Log-Log plot of the core-field ratio of magnetic-shear energy to potential-field energy WL_{SSED}/WL_{SPED} versus the flux content Φ. The [Log Φ, Log (WL_{SSED}/WL_{SPED})] pair of measured values from each magnetogram is plotted as a cross, the spans of which are the 1-σ uncertainties in the measured values. The cloud of 44 crosses has a flat top. The horizontal red line marks the level in the cloud at which the value of an active region's core-field energy ratio is 1. In all of the active regions along the top of the cloud the core-field energy ratio is less than 2. All of the crosses that are within a factor of 2 of the unity line are red in Figure 5. That is, the red crosses in Figure 5 are those of the 44 crosses that have $WL_{SSED}/WL_{SPED} > 0.5$. There are 23 red crosses (23 active regions) in this upper band of the cloud.

The above aspects of the [Log Φ, Log (WL_{SSED}/WL_{SPED})] plot in Figure 5 show that active regions have an upper limit to their core-field ratio of magnetic-shear energy to potential-field energy that is roughly the same for active regions of all sizes in flux content, and that the limiting value of this core-field energy ratio is of order 1. Provided that the core-field energy ratio WL_{SSED}/WL_{SPED} is of the order of the ratio of free energy to potential-field energy for the entire magnetic field of an active region, Figure 5 indicates that an active region of any magnetic size Φ has an upper limit to its free magnetic energy that is of the order of the non-free magnetic energy of its potential field.

6.2. Test of Our Hypothesis

Our hypothesis is that in active regions near the free-energy limit line in (Log $^L\Phi$, Log $^LWL_{SG}$) phase space in Figure 4, the free magnetic energy is of order the non-free energy the field would have were it relaxed to the potential field. By this hypothesis, provided the core-field
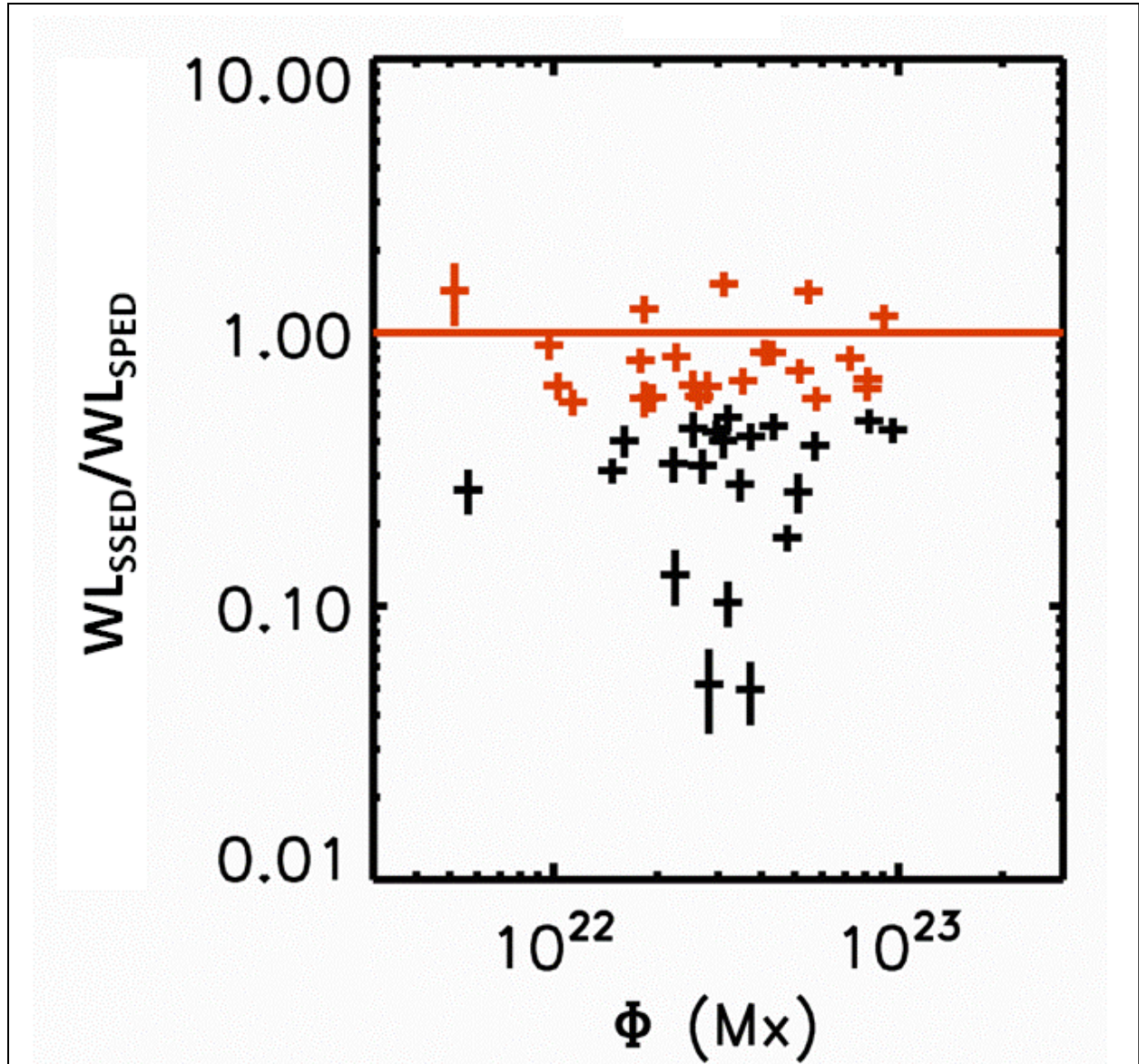
Figure 5. The core-field energy-ratio limit for active regions. The data points are from the MSFC vector magnetograms of the 44 active regions of the Falconer et al (2009) paper. The red crosses are the points that are within a factor of 2 of the unity line. See the text.

energy ratio WL_{SSED}/WL_{SPED} is of order the ratio of free energy to potential-field energy for the whole active region, the top 23 active regions in the [Log Φ, Log (WL_{SSED}/WL_{SPED})] phase space in Figure 5 should be on and near the main sequence of explosive active regions in Figure 4. That is, according to our hypothesis, the flat upper edge of the cloud of 44 [Log Φ, Log (WL_{SSED}/WL_{SPED})] points in Figure 5 should correspond to the slanted upper edge of the cloud of 1800 (Log $^{\llcorner}\Phi$, Log $^{\llcorner}WL_{SG}$) points in Figure 4.

Figure 6 shows the location of the top 23 active regions of Figure 5 in the (Log $^{\llcorner}\Phi$, Log $^{\llcorner}WL_{SG}$) phase space of Figure 4. The blue cloud of (Log $^{\llcorner}\Phi$, Log $^{\llcorner}WL_{SG}$) points in Figure 6 is the same as that in Figure 4. In Figure 6, for each of the top 23 active regions of Figure 5, the (Log $^{\llcorner}\Phi$, Log
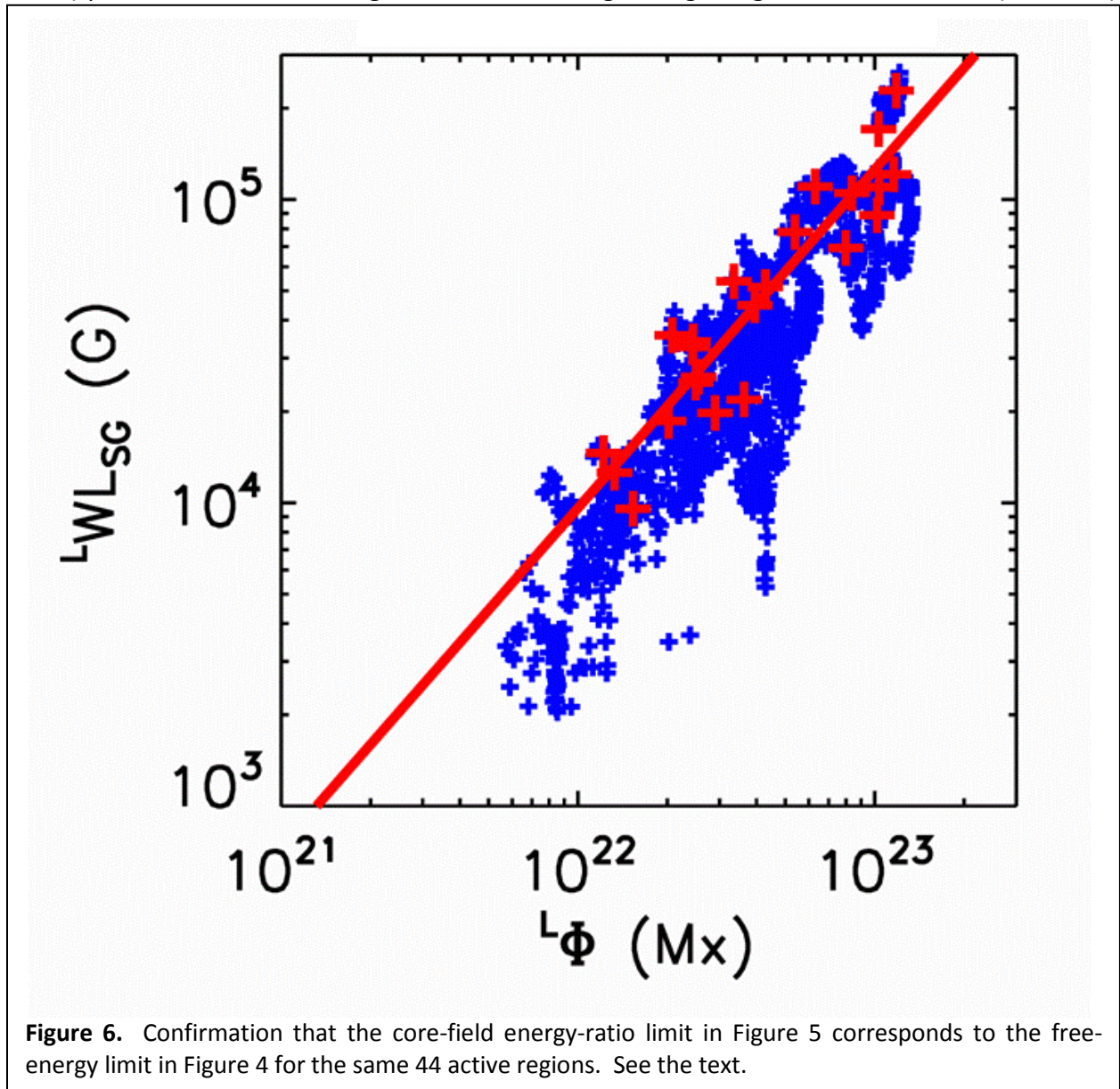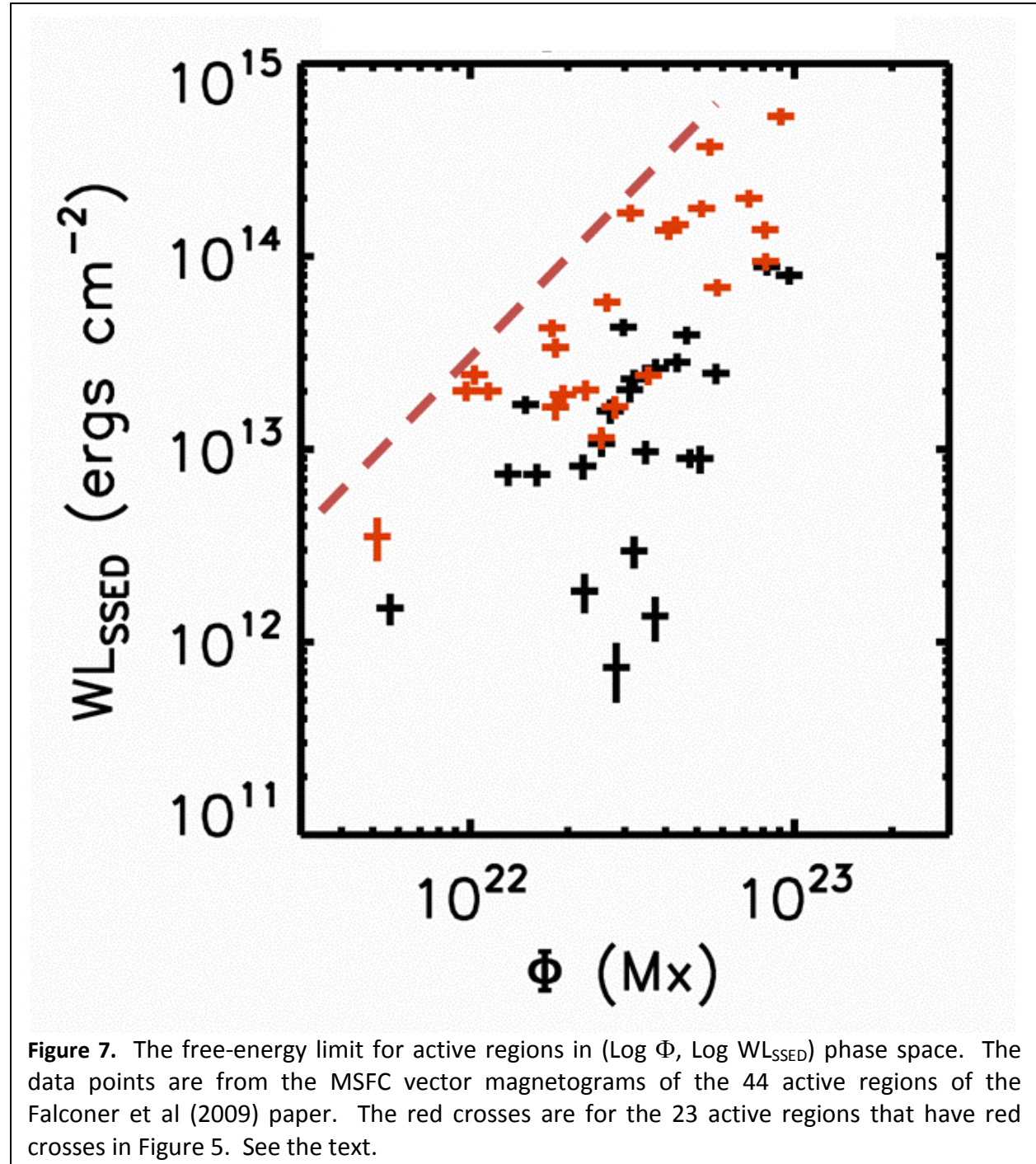
Figure 6. Confirmation that the core-field energy-ratio limit in Figure 5 corresponds to the free-energy limit in Figure 4 for the same 44 active regions. See the text.

to the active region's MSFC vector magnetogram measured for Figure 5 is marked by a red cross. The 23 red crosses are scattered along the path of the main sequence of explosive active regions, the center-line of which path we take to be the CME-fit line in Figure 4. The red line in Figure 6 is the least-squares linear fit to the 23 red crosses. This line runs about as parallel to the upper edge of the blue cloud and about as close to the upper edge as the CME-fit line in Figure 4. Thus, as we expected from our hypothesis, the upper edge of the cloud of points in Figure 5 matches the upper edge of the cloud of points in Figure 4.

The above aspects of Figure 6, together with Figure 5, support our hypothesis. These plots indicate that active regions of all sizes on the explosive main sequence have a uniform magnetic condition that makes them explosive enough to limit their free magnetic energy. They show that this limiting condition occurs when the magnetic-shear energy in the core field increases to

of order the non-free energy in the core of the active region's potential field. This result is

Figure 7. The free-energy limit for active regions in (Log Φ, Log WL_{SSED}) phase space. The data points are from the MSFC vector magnetograms of the 44 active regions of the Falconer et al (2009) paper. The red crosses are for the 23 active regions that have red crosses in Figure 5. See the text.

consistent with either of two possibilities. One possibility is that the limiting condition ($WL_{SSED}/WL_{SPED} \sim 1$) found from measuring the core field makes the core field itself explosive enough to limit the active region's free energy. The other possibility is that this core-field condition reflects a more global condition of the active region's magnetic field (e.g., possibly, as we hypothesize, the entire field's ratio of free energy to potential-field energy is ~ 1 when

$WL_{SSED}/WL_{SPED} \sim 1$), and the global condition makes the entire field explosive enough to limit the field's free energy when $WL_{SSED}/WL_{SPED} \sim 1$.

6.3. Core-Field Magnetic-Shear Energy Limit

As we discussed in Section 5, because the neutral-line magnetic measure WL_{SSED} is similar to WL_{SS} and WL_{SS} is evidently a proxy measure of the free energy of an active region's entire magnetic field, WL_{SSED} should be at least as good a free-energy proxy as WL_{SS}. By its construction, WL_{SSED} should be an even better proxy measure of the magnetic-shear energy in an active region's core field. If these expectations are true, then for the 44 active regions measured for the phase-space plots in Figures 4 and 5, plotting these active regions in (Log Φ, Log WL_{SSED}) phase space should give a cloud of points that has a slanted upper edge, displaying the same free-energy limit that is shown by the slanted upper edge of the blue cloud of (Log $^{\llcorner}\Phi$, Log $^{\llcorner}WL_{SG}$) points in Figures 4 and 6.

Figure 7 shows the plot of the (Log Φ, Log WL_{SSED}) points (crosses) measured from the deprojected vector magnetograms of the 44 active regions. This cloud of 44 (Log Φ, Log WL_{SSED}) points is similar to the cloud of 1800 (Log $^{\llcorner}\Phi$, Log $^{\llcorner}WL_{SG}$) points in Figures 4 and 6 in that it has a roughly linear slanted upper edge. The slope of the upper edge in Figure 7 is approximately the slope of the red dashed straight line. The slope is about 1.8, showing that in this phase space the free-energy-limit upper edge of the distribution of active regions is steeper than in the (Log $^{\llcorner}\Phi$, Log $^{\llcorner}WL_{SG}$) phase space of the plots in Figures 4 and 6. The red crosses in Figure 7 are for the top 23 active regions in Figure 5, the active regions having the 23 highest values of the core-field energy ratio WL_{SSED}/WL_{SPED}. All of the crosses on the upper edge of the cloud are red, showing that these active regions all have core-field energy ratios WL_{SSED}/WL_{SPED} that are of order 1.

The above features of the (Log Φ, Log WL_{SSED}) plot in Figure 7, by corroborating our claim that $^{\llcorner}WL_{SG}$, WL_{SS}, and WL_{SSED} are comparable free-energy proxies, lend further support to our hypothesis that the underlying cause of the free-energy limit and explosive main sequence of active regions is the steeply increasing explosiveness of the field when the free magnetic energy in the entire field or at least in the core field increases to of order the potential-field energy. Independently of whether our hypothesis is true, Figure 7 directly shows that there is an upper limit to the core-field magnetic-shear energy an active region can attain and that this limit is higher for active regions of greater flux content.

7. CONCLUSION

From Figures 4, 5, 6, and 7 together, we conclude that there is an upper limit to the magnetic-shear energy in an active region's core field, and that the limit is of order the non-free magnetic energy that the core field would have were the active region's entire field relaxed to the potential field. We also conclude from these Figures that our proxy measure of the core field's ratio of magnetic-shear energy to potential-field energy WL_{SSED}/WL_{SPED} is plausibly of

order the ratio of free energy to potential-field energy for the active region's entire magnetic field.

Evidently, as an active region's core-field magnetic-shear energy approaches the level of the non-free magnetic energy in the core of the potential field, the explosiveness of the active region's field increases steeply, and the resulting steep increase in the rate of depletion of the field's free energy keeps the free energy from rising much above that level. This results in both the free-energy-limit upper edge of the distribution of active regions in (flux content, free-energy proxy) phase space and the main sequence of explosive active regions bordering the upper edge.

In Figure 7, the crosses closest to the upper edge of the cloud of (Log Φ, Log WL_{SSED}) points are all red, showing that these active regions have $WL_{SSED}/WL_{SPED} > 0.5$. Farther from the upper edge, black crosses are mixed together with red crosses. Still farther from the upper edge, there are only black crosses of active regions having $WL_{SSED}/WL_{SPED} < 0.5$. We interpret this progression with distance through the cloud from its free-energy-limit upper edge as follows. When an active region's core-field energy ratio WL_{SSED}/WL_{SPED} is much less than 1, the active region's magnetic field is incapable of being triggered to explode. As the core-field energy ratio begins to approach 1, rising to 0.5 or so, the field becomes less stable. It becomes capable of being triggered to explode, but only by infrequently occurring special conditions of the field's structure and/or evolution. Finally, when the core-field energy ratio is 1 or greater, practically any perturbation can trigger the field to explode. That is, when the core-field energy ratio is 1 or greater, the active region's field is compelled to explode. This keeps the core-field ratio of magnetic-shear energy to potential-field energy from getting much above 1, and probably keeps an active region's entire field from having free energy that is much more than the non-free energy of the potential field.

REFERENCES

Antiochos, S. K. 1998, ApJ, 502, L181.

Aulanier, G., Torok, T., Demoulin, P., & DeLuca, E. E. 2010, ApJ, 708, 314.

Canfield, R. C., Hudson, H. S., & McKenzie, D. E. 1999, GRL, 26, 627.

Charbonneau, P. 2005, Living Reviews of Solar Physics, 2, 2 (online article, http://www.livingreviews.org/lrsp-2005-2).

Cowling, T. G. 1957, Magnetohydrodynamics (New York: Interscience).

Cui, Y., Li, R., Zhang, L., He, Y., & Wang, H. 2006, Sol. Phys., 237, 45.

Falconer, D. A. 2001, JGR, 106 (A11), 25185.

Falconer, D. A., Moore, R. L., & Gary, G. A. 2002, ApJ, 569, 1016.

Falconer, D. A., Moore, R. L., & Gary, G. A. 2003, JGR, 108 (A10), 1380.

Falconer, D. A., Moore, R. L., & Gary, G. A. 2006, ApJ, 644, 1258.

Falconer, D. A., Moore, R. L., & Gary, G. A. 2008, ApJ, 689, 1433.

Falconer, D. A., Moore, R. L., Gary, G. A., & Adams, M. 2009, ApJ, 700, L166.

Fan, Y., Zweibel, E. G., Linton, M. G., & Fisher, G. H. 1999, ApJ, 521, 460.

Forbes, T. G. 2000, JGR, 105, 23153.

Gary, G. A., Moore, R. L., Hagyard, M. J., & Haisch, B. M. 1987, ApJ, 314, 782.

Georgoulis, M. K., & Rust, D. M. 2007, ApJ, 661, L109.

Gibson, S. E., Fan, Y., Mandrini, C., Fisher, G., & Demoulin, P. 2004, ApJ, 617, 600.

Gopalswamy, N., Mewaldt, R., & Torsti, J. (eds.) 2006, Solar Eruptions and Energetic Particles (Washington, DC: AGU).

Heyvaerts, J., Priest, E. R., & Rust, D. M. 1877, ApJ, 216, 123.

Hirayama, T. 1974, Sol. Phys., 34, 323.

Jing, J., Song, H., Abramenko, V., Tan, C., & Wang, H. 2006, ApJ, 644, 1273.

Klimchuk, J. A., 2001, in Space Weather, ed. P. Song, H. J. Singer, & G. L. Siscoe (Washington, DC: AGU), 143.

Kopp, R. A., & Pneumann, G. W. 1976, Sol. Phys., 50, 85.

Leka, K. D., & Barnes, G. 2003a, ApJ, 595, 1277.

Leka, K. D., & Barnes, G. 2003b, ApJ, 595, 1296.

Low, B. C., 1982, Sol. Phys., 77, 43.

Lynch, B. J., Antiochos, S. K., DeVore, C. R., Luhmann, J. G., & Zurbuchen, T. H. 2008, ApJ, 683, 1192.

Moore, R. L. 1992, in The Astronomy and Astrophysics Encyclopedia, ed. S. P. Maran (New York: Van Nostrand Reinhold), 637.

Moore, R. L., Hagyard, M. J., & Davis, J. M. 1987, Sol. Phys., 113, 347.

Moore, R. L., & LaBonte, B. J. 1980, in Solar and Interplanetary Dynamics, ed. M. Dryer & E. Tandberg-Hanssen (Dordrecht: Reidel), 207.

Moore, R., & Rabin, D. 1985, ARAA, 23, 239.

Moore, R. L., & Roumeliotis, G. 1992, in Eruptive Solar Flares, ed. Z. Svestka, B. V. Jackson, & M. E. Machado (Berlin: Springer), 69.

Moore, R. L., & Sterling, A. C. 2006, in Solar Eruptions and Energetic Particles, ed. N. Gopalswamy, R. Mewaldt, & J. Torsti (Washington, DC: AGU), 43.

Moore, R. L., Sterling, A. C., & Suess, S. T. 2007, ApJ, 668, 1221.

Moore, R. L., Sterling, A. C., Gary, A. G., Cirtain, J. W., & Falconer, D. A. 2011, Space Sci. Rev., in press.

Moore, R. L., Sterling, A. C., Hudson, H. S., & Lemen, J. R. 2001, ApJ, 552, 833.

Qiu, J., Wang, H., Cheng, C. Z., & Gary, D. E. 2004, ApJ, 604, 900.

Roussev, I. I., Forbes, T. G., Gombosi, T. I., Sokolov, I. V., De Zeeuw, D. I., & Brin, J. 2003, ApJ, 588, L45.

Rust, D. M., & Kumar, A. 1996, ApJ, 464, L199.

Schrijver, C. J. 2007, ApJ, 655, L117.

Shibata, K. 1998, in Observational Plasma Astrophysics: Five Years of Yohkoh and Beyond, ed. T. Watanabe, T. Kosugi, & A. C. Sterling (Dordrecht: Kluwer), 187.

Shibata, K., Masuda, S., Shimojo, M., Hara, H., Yokoyama, T., Tsueta, S., Kosugi, T., & Ogawara 1995, ApJ, 451, L83.

Sterling, A. C., Hudson, H. S., Thompson, B. J., & Zarro, D. M. 2000, ApJ, 532, 628.

Sturrock, P. A., Kaufman, P., Moore, R. L., & Smith, D. F. 1984, Sol. Phys., 94, 341.

Tanaka, K. 1991, Sol. Phys., 136, 133.

Wang, H. 2006, ApJ, 649, 490.

Zirin, H. 1988, Astrophysics of the Sun (Cambridge: Cambridge University Press).

Zirin, H., & Liggett, M. A. 1987, Sol. Phys., 113, 267.